Evaluation of the Timing Performance of the ATLAS LAr Calorimeter Digital Trigger (DT)

Amalia Tsitsekli, CERN Summer Student

CERN, Geneva, Switzerland

August 12, 2025

Abstract

The ATLAS Liquid Argon calorimeter provides energies to the first level calorimeter trigger at 40 MHz with high granularity, relying on a good timing performance to correctly identify the bunch crossing from which the energy deposits originate. Using a calibration dataset, I quantify the intrinsic timing of electromagnetic super-cells, compare three reference-time definitions derived from the main readout cell times, and study the resolution. The energy-weighted cell average yields the sharpest $\Delta t = t_{\mathrm{SC}} - t_{\mathrm{ref}}$ core across layers and thresholds. In the electromagnetic barrel Layer 2 the intrinsic resolution improves from about 4.7 ns at 1 GeV to 2 GeV to roughly 0.7 ns above 20 GeV. Residual biases remain within ± 0.5 ns. The results show sub-nanosecond timing resolution for the super cells at moderate energies and provide a baseline for additional digital trigger and trigger timing studies.

1 Introduction and Motivation

The ATLAS Liquid Argon (LAr) calorimeter is esential for the reconstruction of electromagnetic (EM) particles [1] and jets and for providing signals for calorimeter-based online selection of events, called triggering [2, 3]. A new digital trigger (DT) was installed in Long Shutdown 2 [2] to help cope with the increased pileup, allowing the online selection of potentially interesting events with better efficiency compared to the legacy analog trigger [3]. This report evaluates the present DT timing performance using Run 3 data and focuses on (i) comparing reference-time schemes formed from the measurements from the physical calorimeter cells, as calculated on the main read out (ROD) available, (ii) establishing the intrinsic super cell (SC) timing resolution versus energy and layer, (iii) quantifying residual biases, and (iv) using two simple, event shaped measures to investigate the performance of the max energy cell.

2 Dataset and Selections

The study uses one dataset from run `00499666` configured with the `LArPromptAnalysis` framework[4] and reference with both SC cell and ROD quantities available. Events were collected by the LAr Partial Event Building (PEB) stream, which allows for a relatively increased set of information per SC to be recorded, for a subset of triggers. In this analysis, 240166 events were used. The file path is:

```
/eos/atlas/atlastier0/tzero/prod/caf/LAr/data25_13p6TeV/calibration_LArPEBDigitalTrigger/
00499666/.../merge.NTUP_SCMON.c1638_m2220.0201.1       (LArPromptAnalysis)
```

Energies are converted to GeV as follows: SC energies multiplied by 12.5/1000; ROD-cell energies divided by 1000. Selections are made: super-cell energy thresholds at 1 GeV, 2 GeV, 4 GeV, 5 GeV and 10 GeV; per-cell threshold $E_i > 0.2$ GeV when building the reference. Six EM layers are analysed: EM barrel (EMB) and endcap (EMEC), Layers 1–3. Results are presented with a focus on EMB Layer 2, the core shower layer.

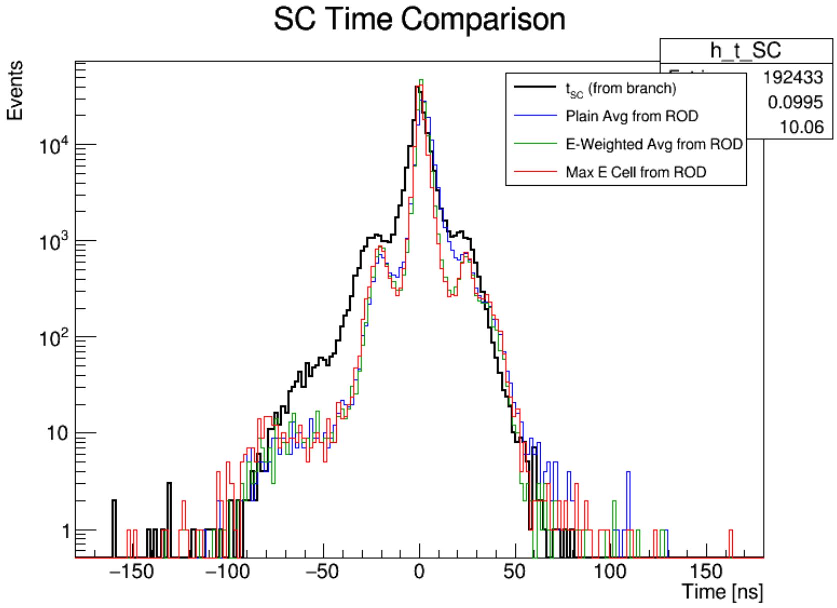

Figure 1: Timing overlay: $t_{\rm SC}$ with the three $t_{\rm ref}$ at $E_{\rm SC} > 1\,\text{GeV}$, $E_i > 0.2\,\text{GeV}$.

3 Methodology

Given an SC time $t_{\rm SC}$ and its N constituent cell times t_i with energies E_i, define

$$\Delta t \;=\; t_{\rm SC} \;-\; t_{\rm ref}\,,$$

with three choices for $t_{\rm ref}$:

1. **Plain average:** $t_{\rm ref} = \frac{1}{N}\sum_{i=1}^{N} t_i$.
2. **Energy-weighted (EW):** $t_{\rm ref} = \dfrac{\sum_i E_i t_i}{\sum_i E_i}$.
3. **Max-energy cell:** $t_{\rm ref} = t_j$ where $E_j = \max\{E_i\}$.

The plain average is simple but sensitive to noisy low-energy neighbours. The max-cell time is attractive for compact EM showers yet unstable for jets or in the presence of glitches. The EW definition balances both effects and, empirically, yields the narrowest Δt core.

For each selection, the distribution of Δt is fitted around the peak to extract the intrinsic width. The Gaussian core fits are applied within $|\Delta t| < 2\,\text{rms}$; the fitted width is quoted as σ_t. The energy dependence is modelled [1] as

$$\sigma_t(E_{\rm SC}) = \sqrt{a^2 + \frac{b^2}{E_{\rm SC}^2}}\,,$$

which captures a constant high-energy floor (a) and a term falling as $1/E$ (b/E).

4 Results

4.1 Overlay of timing schemes

Figure 1 overlays the three reference schemes and the SC time for EMB Layer 2 at $E_{\rm SC} > 1\,\text{GeV}$ and $E_i > 0.2$ GeV. The same generic form is observed for each of the distributions, with the three reference schemes being narrower and the SC time having a wider spread.

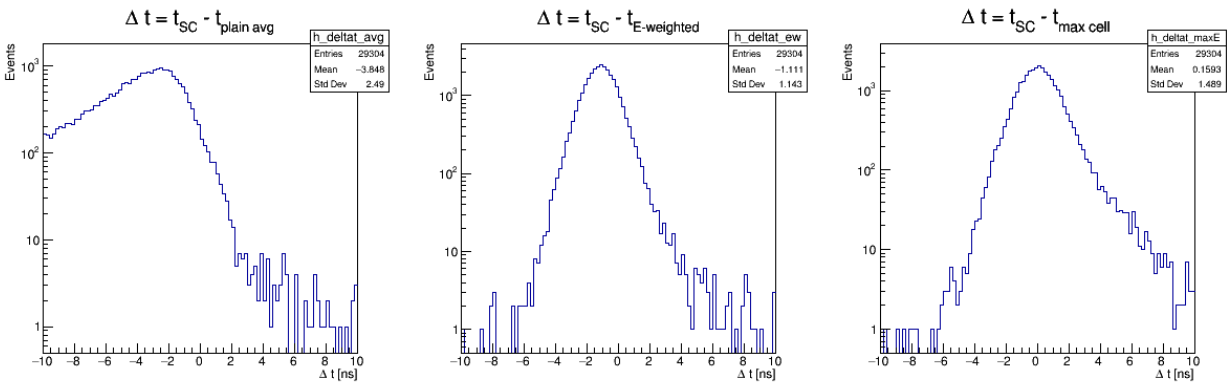

Figure 2: Δt distribution with different reference schemes (plain average, max-energy cell and EW) for EMB Layer 2 at $E_{\mathrm{SC}} > 1\,\mathrm{GeV}$, $E_i > 0.2\,\mathrm{GeV}$. Plain average appears with the worst performance, whereas EW has the narrowest and most symmetrical core.

4.2 Layer comparison and max-cell behaviour

At low energies in EMB, the max-cell reference can be competitive for EM-like events [1]; however, it degrades in EMEC and as the energy threshold increases, where broader shower shapes and neighbour noise become more influential. Across layers, EW delivers the most stable performance. This behavior can be concluded from multiple Δt distributions made across Layers 1–3 of EMB and EMEC for different energy cuts. Figure 2 shows an example of said distributions, comparing plain average, max-energy cell and EW Δt.

4.3 Resolution vs. energy (EMB Layer 2)

Using the EW reference, the intrinsic resolution improves from $\sim 4.7\,\mathrm{ns}$ in the $1\,\mathrm{GeV}$ to $2\,\mathrm{GeV}$ bin to about $\sim 0.7\,\mathrm{ns}$ above $20\,\mathrm{GeV}$. This energy scaling and constant floor are consistent with LAr timing measurements [1]. Fitting $\sigma_t(E) = \sqrt{a^2 + (b^2/E^2)}$ returns

$$a = 0.6992 \pm 0.0410\,\mathrm{ns}, \qquad b = 7.7626 \pm 1.4744\,\mathrm{ns\,GeV}, \qquad \chi^2 = 0.43\,.$$

Figure 3 shows the extracted points and the fit curve.

Comparing it to the intrinsic resolution of t_{SC}, Δt provides better resolution overall, by getting rid of some correlated bias components.

Figure 4 shows the extracted points and the fit curve for t_{SC}. The high energy constant is bigger then for the Δt intrinsic resolution ($a = 0.7643 \pm 0.0466\,\mathrm{ns}$).

4.4 Biases and gain-scale effects

The mean offset $\langle \Delta t \rangle$ presents a stable within $\pm 0.5\,\mathrm{ns}$ behavior for Layer 2. When using the *plain* SC time (instead of EW Δt), the mean vs. energy exhibits a residual bias pattern. This correlates with the main-readout changes of the gain scale [3] at higher energies as shown in figure 5; by construction, Δt removes part of this correlated component, delivering a flatter bias and better overall resolution, notably above $5\,\mathrm{GeV}$. An example trend is shown in figure 6.

5 Investigation of the performance of the maxEcell

As can be observed, the most energetic cell is not performing very well as a reference for the true time of the energy deposition in the SC. A study is conducted to investigate whether jet events are dominating, and therefore the most energetic cells' use is not motivated. The most energetic cell in the middle Layer of every EM cluster is used in standard ATLAS reconstruction to define the time of arrival of electrons and photons [1]. As this algorithm might not be expected to perform well

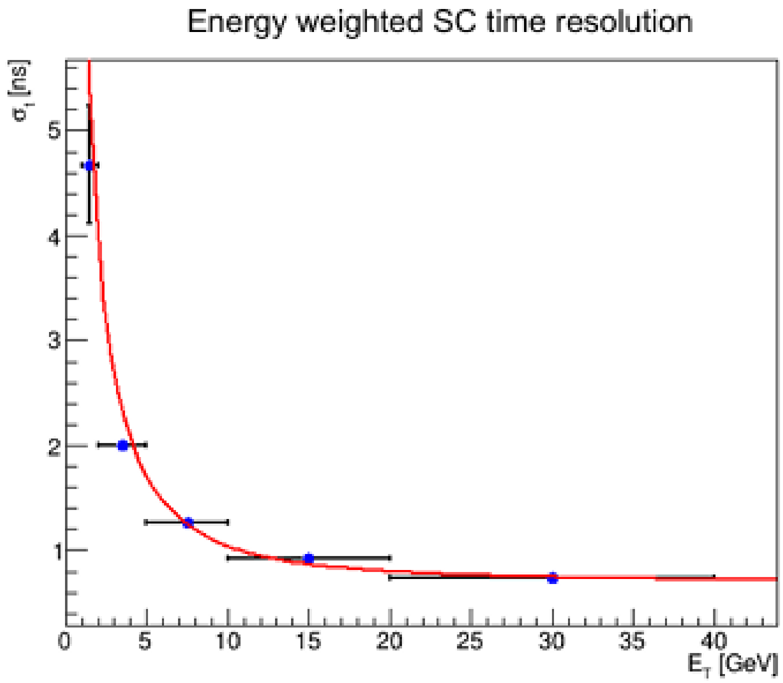

Figure 3: Intrinsic timing resolution σ_t vs. E_{SC} of Δt in EMB Layer 2 (EW reference) with fit $\sqrt{a^2 + (b^2/E^2)}$.

for jets, we wanted to see if we could easily separate SC time measurements based on their energy spread.

Two methods were explored to separate two classes of events, namely well defined single cell energy deposits in the SC (photon or electron hitting the calorimeter) or more energy spread (jets):

$$\frac{\sigma_E}{E_{\mathrm{SC}}} = \frac{\sqrt{\frac{1}{N}\sum_i (E_i - \bar{E})^2}}{E_{\mathrm{SC}}} \quad \text{(cell-energy spread)}, \tag{1}$$

$$\frac{\Delta E}{E_{\mathrm{SC}}} = 1 - \frac{E_{\max}}{E_{\mathrm{SC}}} \quad \text{(core-energy fraction)}. \tag{2}$$

Distributions for EMB Layers 1–3 at $E_{\mathrm{SC}} > 1\,\mathrm{GeV}$, $5\,\mathrm{GeV}$ and $10\,\mathrm{GeV}$ show: (i) low-E_{T} SCs have the narrowest spread; (ii) as E_{T} rises, σ_E/E_{SC} remains in the rough range 0–0.5 across layers; (iii) L1 is tightest at low energy, while L3 retains a slightly narrower spread above 5 GeV. Crucially, neither variable yields a clean class separation on this dataset. Figure 7 illustrates $\Delta E/E_{\mathrm{SC}}$ and figure 8 $\frac{\sigma_E}{E_{\mathrm{SC}}}$ for EMB Layer 2.

6 Conclusion and Outlook

The EW reference provides a practical compromise: it suppresses small-energy neighbours, avoids reliance on a single hottest cell, and improves both the core width and tails of Δt. The fitted constant term of $\sim 0.70\,\mathrm{ns}$ sets a plausible high-energy floor, with the b/E term dominating in the few-GeV regime. However, using the main readout time as reference is not very promising, at least not while using simply the time from the cells relevant to each SC. The online ROD time offers a good starting point, but not equivalent to the <200 ps threshold needed to establish a good reference time for the collision [1, 5]. The two event-shape measures did not yield a clear class separation in this sample.

Next steps would include validating performance under higher pile-up, and testing multiple configured datasets, and performing calibration to improve the instrinsic time resolution.

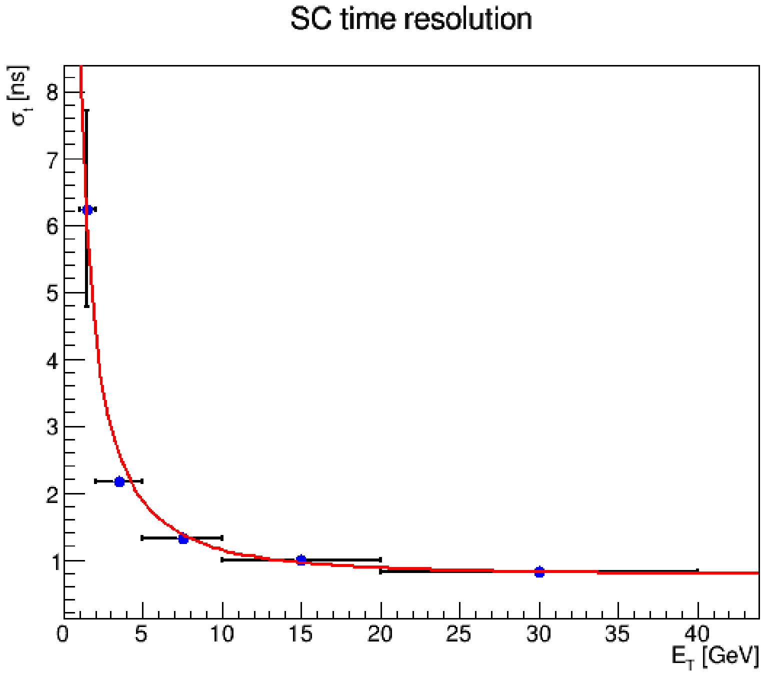

Figure 4: Intrinsic timing resolution σ_t vs. E_{SC} of t_{SC} in EMB Layer 2. Fitting $\sqrt{a^2 + (b^2/E^2)}$ returns $a = 0.7643 \pm 0.0466\,\mathrm{ns}$ and $b = 8.5860 \pm 1.7985\,\mathrm{ns\,GeV}$.

Acknowledgements

I want to thank my supervisor Nikiforos, and the ATLAS LAr community for their guidance and feedback, as well as the CERN Summer Student Programme firstly for their support and secondly for the great experience.

References

[1] M. Aharrouche, J. Colas, L. Di Ciaccio, et al. Time resolution of the atlas barrel liquid argon electromagnetic calorimeter. *Nucl. Instrum. Methods A*, 597:178–188, 2008.

[2] Atlas liquid argon calorimeter phase-i upgrade: Technical design report. Technical Report CERN-LHCC-2013-017, ATLAS-TDR-022, CERN, 2013.

[3] The phase-i trigger readout electronics upgrade of the atlas liquid argon calorimeters. *JINST*, 17:P05024, 2022.

[4] ATLAS LAr DQ Experts. Ladies investigation. `https://gitlab.cern.ch/atlas-lar-dq-experts/ladies-investigation`, 2025. GitLab repository; version main.

[5] N. J. Buchanan et al. Atlas liquid argon calorimeter front end electronics. *JINST*, 3:P03004, 2008.

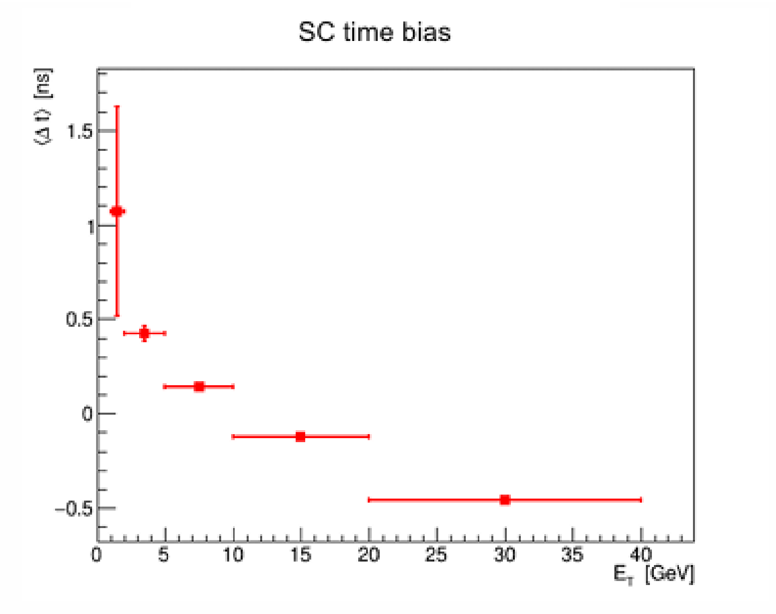

Figure 5: Example mean timing bias $\langle\ t\rangle$ vs. E_{SC} in EMB Layer 2. The SC time t_{SC} presents a gain-related bias.

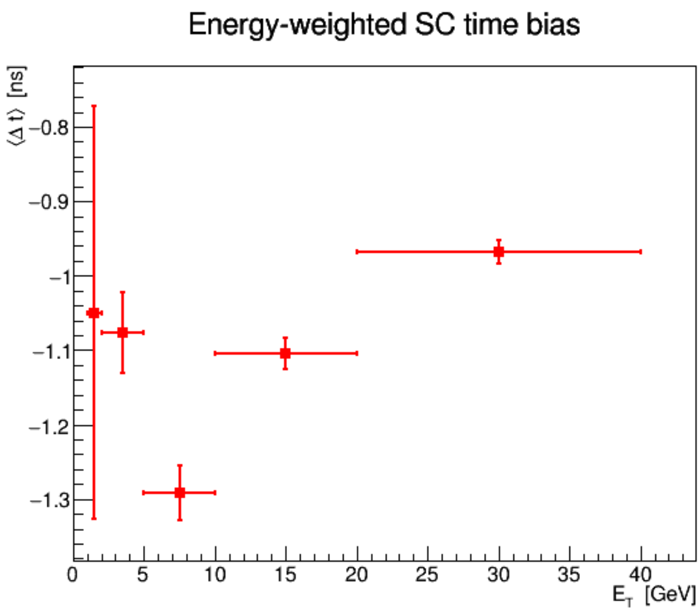

Figure 6: Example mean timing bias $\langle\Delta t\rangle$ vs. E_{SC} in EMB Layer 2. The energy-weighted Δt mitigates gain-related bias seen when using the plain SC time.

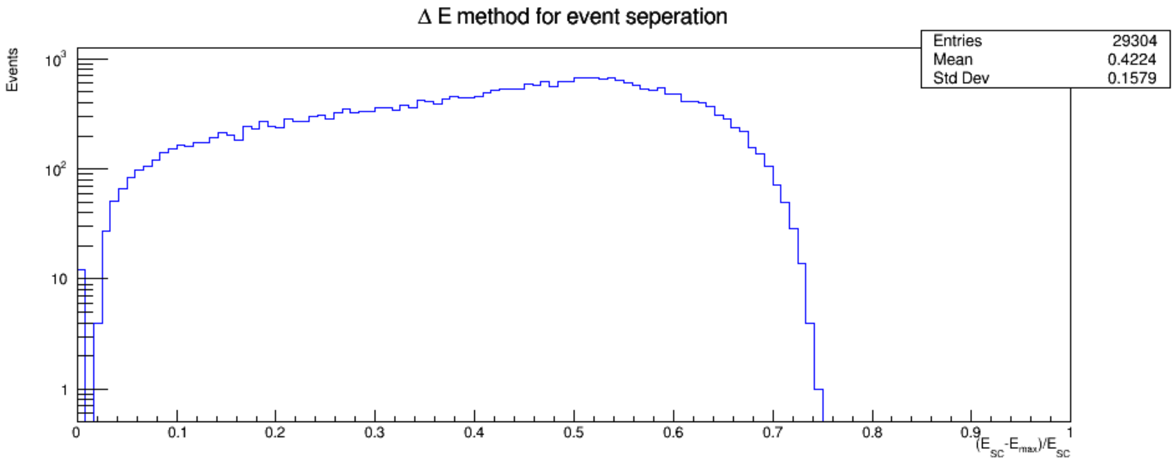

Figure 7: $\Delta E/E_{\mathrm{SC}}$ in EMB Layer 2 at $E_{\mathrm{SC}} > 5\,\mathrm{GeV}$. No strong class separation is observed.

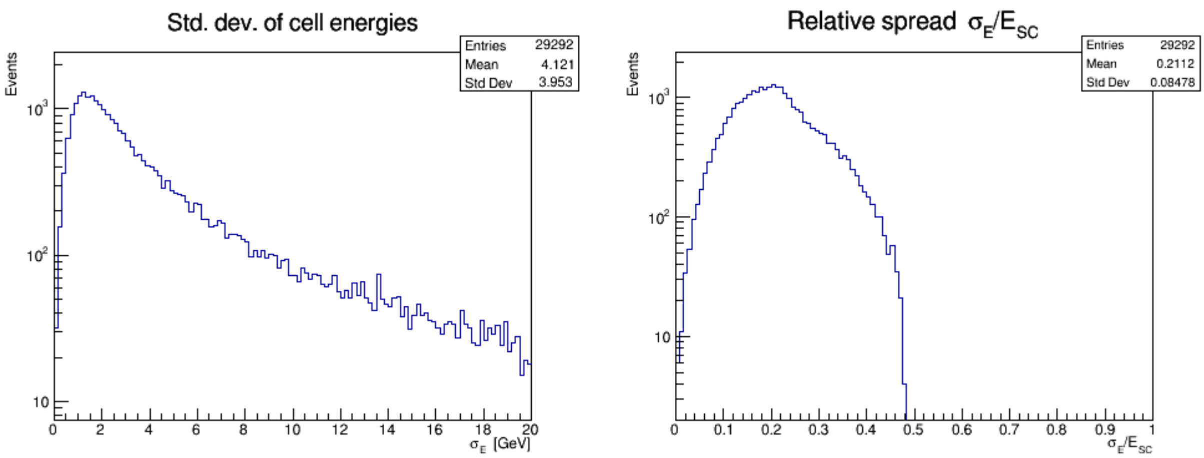

Figure 8: $\frac{\sigma_E}{E_{\mathrm{SC}}}$ in EMB Layer 2 at $E_{\mathrm{SC}} > 5\,\mathrm{GeV}$. No strong class separation is observed.